

Sensitivity of Headland Bypassing to Variations in Local Wave Conditions and Regional Climate Drivers

Daniel Wishaw¹, Javier Xavier Leon¹, Thomas Robert Mortlock², Matthew Barnes³, and Guilherme Vieira da Silva⁴

¹University of the Sunshine Coast

²Aon Reinsurance Solutions

³BMT Commercial

⁴Griffith University

June 8, 2023

Abstract

Headland sediment transport is dynamic and complex, but understanding the transport mechanisms is necessary for effective long-term management of downdrift beach compartments. In this study, we have develop a coastal process model using TUFLOWFV, that is used to calibrate an approximation tool for headland bypassing at the study site. The approximation tool is shown to reproduce sediment transport rates at the headland apexes accurately and efficiently. We have explored the headland sediment transport mechanism, the influence of wave height and direction, and the sensitivity in regional climate conditions. Headland sediment transport is shown to occur as ‘trickle’ bypassing under modal wave conditions or ‘sand slug’ migration under storm wave conditions that travel in either a headland-attached and a cross-embayment pathway. Bypassing during storm wave conditions produces 50% to 60% of total bypassing volume, despite only accounting for 6% of the recorded days. The results indicate that headland transport is sensitive to changes in wave direction and wave height, with the existing mean wave direction balancing sediment transport on the east and north faces of the headland. Seasonality is the most significant climatic control on headland transport, while ENSO phase is only significant for the headland apexes that are exposed to south-east wave conditions. The potential for anticlockwise rotation of the wave climate in future is explored, with greater erosion of the northern beaches of the headland likely due to a reduced supply of sediment around the eastern point of the headland and greater erosive wave power on the north side.

Hosted file

962267_0_art_file_10941333_rvr5vq.docx available at <https://authorea.com/users/626513/articles/647889-sensitivity-of-headland-bypassing-to-variations-in-local-wave-conditions-and-regional-climate-drivers>

18 Abstract

19 Headland sediment transport is dynamic and complex, but understanding the transport mechanisms is necessary for
20 effective long-term management of downdrift beach compartments. In this study, we have develop a coastal process
21 model using TUFLOWFV, that is used to calibrate an approximation tool for headland bypassing at the study site.
22 The approximation tool is shown to reproduce sediment transport rates at the headland apexes accurately and
23 efficiently. We have explored the headland sediment transport mechanism, the influence of wave height and
24 direction, and the sensitivity in regional climate conditions. Headland sediment transport is shown to occur as
25 ‘trickle’ bypassing under modal wave conditions or ‘sand slug’ migration under storm wave conditions that travel in
26 either a headland-attached and a cross-embayment pathway. Bypassing during storm wave conditions produces 50%
27 to 60% of total bypassing volume, despite only accounting for 6% of the recorded days. The results indicate that
28 headland transport is sensitive to changes in wave direction and wave height, with the existing mean wave direction
29 balancing sediment transport on the east and north faces of the headland. Seasonality is the most significant climatic
30 control on headland transport, while ENSO phase is only significant for the headland apexes that are exposed to
31 south-east wave conditions. The potential for anticlockwise rotation of the wave climate in future is explored, with
32 greater erosion of the northern beaches of the headland likely due to a reduced supply of sediment around the eastern
33 point of the headland and greater erosive wave power on the north side.

34 Plain Language Summary

35 We investigated sand movement around a headland, and how it is impacted by waves of different sizes and from
36 different directions. We used Noosa Headland, Australia as our study site, as sand moving around this headland is
37 important for the beach condition of the famous Noosa Main Beach. For average wave size days, we found a slow
38 trickle of sand moves around the headland, however, during larger storm wave conditions, sand was transported in
39 large ‘slugs’ of sand. Regional climate variability, such as El Niño/La Niña cycles, had little impact on the
40 movement of sand around the headland, while the specific wave height and direction of each storm was important.
41 Southeast waves produced the strongest transport on the east side of the headland, but weak transport on the north
42 side, while northeast waves were the opposite. We found that the existing average wave direction produced balanced
43 transport around the headland, while projected future wave conditions are likely to produce unbalanced transport,
44 with more erosion and less sand arriving on the northern side of the headland. This change will impact Noosa Main
45 Beach, where this pattern is likely to lead to sand starvation of this beach in future years.

46 1. Introduction

47 Headlands often force a complex hydrodynamic response to wave, wind and tidal conditions that can make
48 prediction of sediment transport around headlands (headland bypassing) difficult to reliably forecast (King et al.,
49 2021; Vieira da Silva et al., 2018). Research relating to headland bypassing is rapidly expanding (Klein et al., 2020)
50 as more tools become available to coastal researchers such as high quality and frequent aerial or satellite images
51 (Wishaw et al., 2021), easier bathymetric survey collection (Silva et al., 2021) and numerical modelling tools (King
52 et al., 2021; McCarroll et al., 2021; Vieira da Silva et al., 2021; Vieira da Silva et al., 2018). Attempts to parametrize
53 headland bypassing using topographical, bathymetric and sediment parameters have been made, however, the
54 interaction between these features and the forcing wave, wind and tidal conditions results in highly localized results
55 that requires specific investigation, particularly at more complex headlands that are substantially different than those
56 used for the parameterization (George et al., 2015; McCarroll et al., 2021).

57
58 The regional climate drivers that produce local wind and wave conditions are constantly evolving due to both sub-
59 seasonal to decadal climate variability and climate-change-derived long-term influences (Mortlock and Goodwin,
60 2015; Mortlock and Goodwin, 2016). Global changes to the wave climate due to global warming include increased
61 wave power, by 0.4% per year (Reguero et al., 2019), robust changes in annual mean significant wave height and
62 mean wave period of 5–15% and shifts in mean deep-water wave direction of 5–15° by the end of the century
63 (Morim et al., 2019). Changes of this magnitude have been shown to influence longshore transport and headland
64 bypassing rates (Splinter et al., 2012; Vieira da Silva et al., 2021), and is expected where headlands are sensitive to
65 wave direction for bypassing or where bypassing requires sequencing of wave conditions to occur for successful
66 headland bypassing (Wishaw et al., 2021). Further research is required to understand the magnitude of this change
67 on headland bypassing at a local scale and its influence on downdrift beaches, which are often highly desirable
68 beach destinations due to the protection of the headland (Wishaw et al., 2020).

69

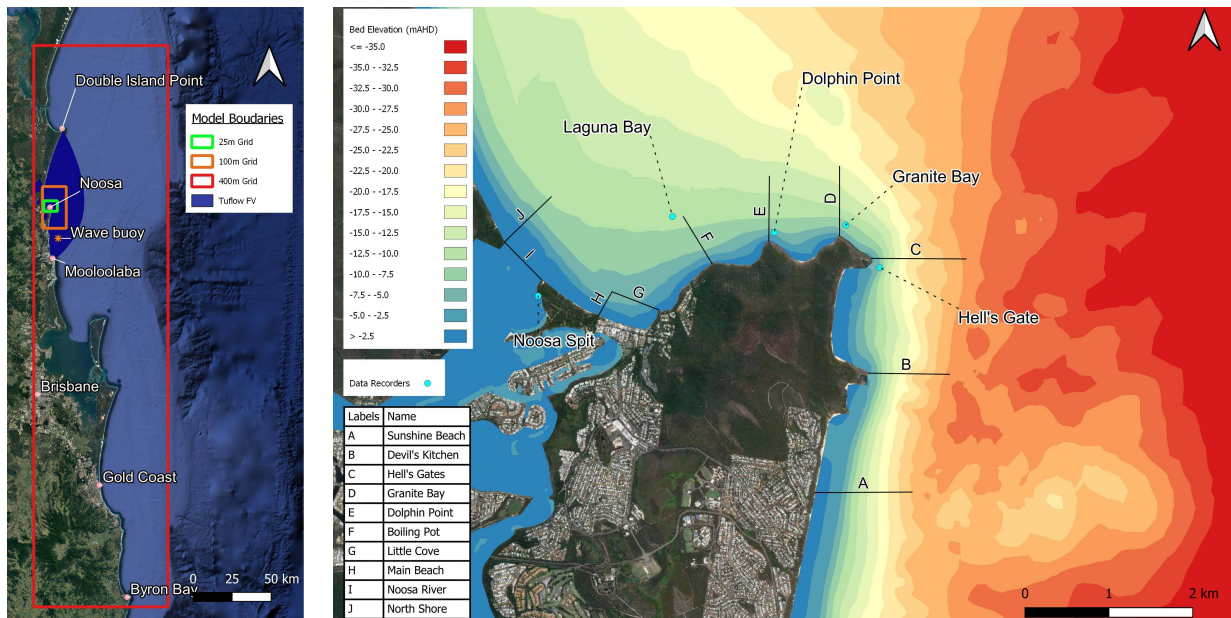
70 To understand local coastal processes and how they may evolve under changing climatic conditions, a range of
 71 process based numerical modelling techniques and tools are available (Deltares, 2022),(BMT Commercial Australia,
 72 2022)). However, due to the computational intensity of these models, they are often prohibitive to use for long term
 73 simulations. Solutions to this include various schematisation of the wave climate to reduce the number of wave
 74 conditions that need to be resolved (Benedet et al., 2016) and the use of process based models to calibrate more
 75 simplistic estimates of sediment transport (Barnes, 2015). Regardless of approach, it is important that coastal
 76 managers and planners have tools that are both flexible and accurate such that they can be applied to both shorter-
 77 term timeframes (weeks-month) and longer-term time frames (years-decades) to help guide management and
 78 planning decisions (Splinter and Coco, 2021).

79
 80 In this study calibrated/validated process-based hydrodynamic, wave and coastal sediment transport models are used
 81 to support the development of an efficient headland bypassing approximation tool. This tool is then used to assess
 82 the sensitivity of headland bypassing to changes in the regional wave conditions associated with plausible future
 83 climate scenarios. The study outputs provide new insights to local headland bypassing that influences the available
 84 sediment supply to the downdrift beaches noted for their high social, recreational and economic value. The tool also
 85 provides a framework for short-, medium- and long-term forecasts of sediment supply which can be used to support
 86 local coastal management decision making and investment.

87 2. Study Area

88 The study location was at Noosa Headland, in Queensland, Australia (**Figure 1**). Noosa Headland is a medium
 89 sized, acute headland with a balanced bathymetric expression (George et al., 2015) that has been used as a study site
 90 for previous work (Wishaw et al., 2021; Wishaw et al., 2020). The open coast shoreline is wave-dominated and
 91 micro-tidal (Harris et al., 2002). The headland contains several small, embayed beaches, with the eastern facing
 92 beach compartments exposed to the dominate modal wave climate and northern facing beaches sheltered from the
 93 modal wave conditions, but exposed to east and northeast wave emanating from tropical lows and (ex) tropical
 94 cyclones in the Coral Sea.

95



96 **Figure 1:** Noosa regional setting with the (a) nested model boundaries shown and (b) the
 97 nearshore bathymetry and headland apices labeled.

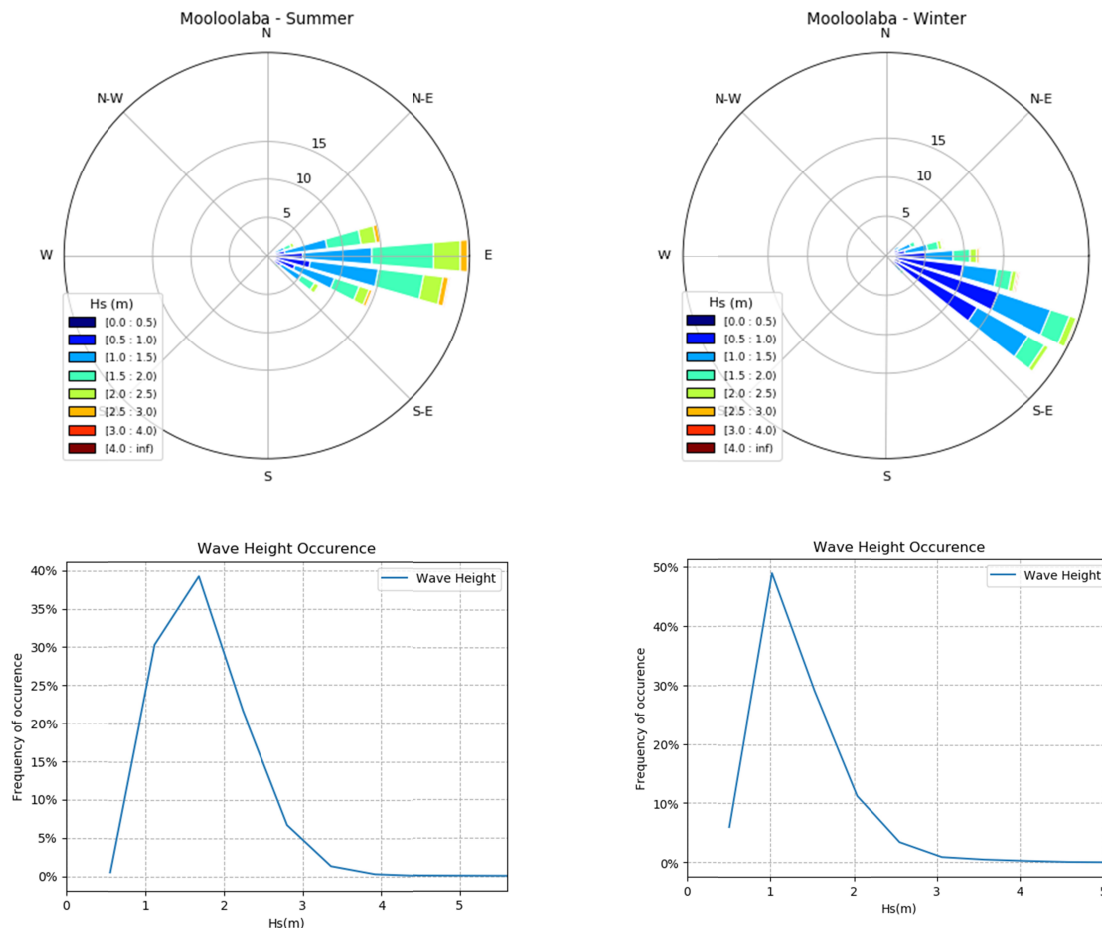
98

99 Wave seasonality at the Mooloolaba wave buoy is defined by larger waves from the east in summer and smaller
 100 waves from the southeast in winter (**Figure 2**) (Barnes et al., 2013). Sites further south show a stronger trend of
 101 winter swell, including waves from the south-southeast direction (Mortlock and Goodwin, 2015), however at
 102 Mooloolaba, protection from Mulgumpin (Moreton Island) and the change in shoreline orientation of the Southern

103 Queensland coast (regionally orientated at 353 degrees true north) compared with the New South Wales coast
 104 (regionally orientated at 12 degrees true north) reduces the exposure to these conditions. Furthermore, the site may
 105 be is also annually exposed to cyclonic wave conditions during the summer originating in the Coral Sea (Wishaw et
 106 al., 2020) which results in increased wave heights and an anti-clockwise rotation of the wave climate in summer.

107
 108 Large wave events ($H_s > 2.5\text{m}$) can occur at the site from both tropical and extra-tropical storm systems, with tropical
 109 systems having a shore normal propagation (easterly) along the coast while extra-tropical storms produce a
 110 shoreline-oblique (southeasterly) propagation (Goodwin et al., 2016). Southeasterly wave conditions tend to drive
 111 sediment transport north along the coastline in the southern extent of the study area, but are generally protected from
 112 influencing the bay beaches on the north side of the headland. In contrast, easterly waves have less impact on long
 113 shore transport on the southern beaches, but drive transport through the bay beaches on the north side of the
 114 headland (Wishaw et al., 2021). Outside of these storm conditions, the modal wave climate along the east coast of
 115 Australia is dominated by a range of synoptic patterns forming in the Coral Sea, Tasman Sea and Southern Ocean
 116 that are modulated by the location of the sub-tropical ridge (Mortlock and Goodwin, 2015).

117



118 **Figure 2:** Recorded wave conditions for the austral summer (a) and austral winter (b) and wave
 119 exceedance for austral summer (c) and austral winter (d).

120

121 2.1 Conceptual understanding of bypassing at Noosa Headland

122 Previous research at this site undertook a shoreline change analysis using 60-years of aerial imagery in conjunction
 123 with local directional wave data to develop a preliminary understanding of the mechanism of headland bypassing
 124 (Wishaw et al., 2021). This assessment concluded that episodic headland bypassing was linked to a specific

125 sequence of wave conditions with waves larger than $H_s = 2.5\text{m}$ from the southeast being followed by waves larger
126 than $H_s = 2.5\text{m}$ from the east-northeast. Furthermore, the calculated annual sediment budget ($-8,900\text{m}^3/\text{year}$) of the
127 protected Noosa Main Beach, indicates that it is currently experiencing significant erosion stress, with increased
128 erosion predicted under future climate conditions. Finally, this previous work evaluated the correlation between
129 ENSO phasing and beach widths, with exposed eastern beaches having a negative correlation with ENSO phase,
130 while the protected beaches on the north of the headland did not show a significant correlation, due to the reliance of
131 the episodic bypassing.

132 3. Process-based modelling

133 3.1 Model development

134 A SWAN (wave) and TUFLOW FV (coastal hydrodynamics and sediment transport) model combination was used
135 to simulate the coastal processes at Noosa Headland (**Figure 1**). SWAN is a third-generation phase-averaged wave
136 model based on fully spectral representation of the action balance equation, accounting for wave-current interaction
137 through radiation stress, refraction, wind generation, whitecapping, nonlinear wave-wave interactions, bottom
138 dissipation, and depth-induced breaking (Delft University of Technology, 2016). The SWAN model for the study
139 area was previously developed and calibrated (Wishaw et al., 2020), and comprises the system of nested grids
140 shown in **Figure 1**. Waves in the nearshore areas around Noosa Headland are resolved at 25m resolution (from the
141 shoreline to approximately 35m depth), with the deeper water conditions sufficiently captured at lower resolution.
142 using three nested grids that step down from a 400m grid that extends to the continental shelf, a 100m regional grid
143 and a 25m grid in the study area. The nested wave models utilize water level outputs from the hydrodynamic model
144 that are passed through to SWAN from TUFLOW FV after simulating tide, wind, and mean sea level pressure to
145 ensure accuracy of the wave interaction with the seabed in shallow water.

146
147 TUFLOW FV is a flexible mesh finite volume numerical model that solves the conservative integral form of the
148 nonlinear shallow water equations to simulate hydrodynamics, sediment transport and water quality processes in 3d
149 or in a depth averaged 2d and 1d modes (BMT Commercial Australia, 2022). For this research, hydrodynamics and
150 sediment transport modules were utilized in a depth averaged 2d configuration . The model mesh resolution varies
151 from 1900m grid at the offshore boundary grid that was downscaled to a $\sim 50\text{m}$ grid in the nearshore area of interest
152 (where higher rates of sediment transport are typically observed). The model mesh resolution smoothly downscales
153 using triangular and quadrilateral cells.

154
155 Bathymetry inputs for the model utilized the same combination of inputs as per the SWAN model, which are defined
156 through a combination of the following datasets: i) a 2m resolution Digital Elevation Model (DEM) created from a
157 hydrographic survey of the lower Noosa river and parts of Laguna Bay; ii) , a 2011 bathymetric LiDAR survey of
158 the Sunshine Coast (Queensland Government, 2012) extending from the shoreline to $\sim 20\text{m}$ depth ; iii) and a high-
159 resolution (30m) depth model for the Great Barrier Reef in areas further offshore (Geoscience Australia, 2017).

160
161 Spatially and temporally varying wind field and mean sea level pressure inputs are derived from the NOAA CFSR
162 and CFSv2 global model datasets (Saha, 2014; Saha, 2006). The tidal water level variation used to define the
163 hydrodynamic model offshore boundary is based on Mooloolaba Tide gauge recordings (Queensland Government,
164 2019a) and scaling developed as part of the model calibration process. The wave model offshore boundary (applied
165 at the eastern boundary of the 400m grid) is defined using nonstationary peak wave parameters derived from the
166 Mooloolaba Wave buoy recordings (Queensland Government, 2019b) and deep water wave transformation.

167
168 Non-cohesive coastal sediment transport is modelled following (Van Rijn, 2007a; Van Rijn, 2007b; Van Rijn,
169 2007c) as implemented within TUFLOW FV, allowing simulation of multiple fraction sediment transport including
170 wave- and current-related bedload and suspended load. The presence of waves can enhance sediment pickup and
171 therefore also the rate of transport by the local currents. The prediction of wave-related sediment transport due to
172 processes such as wave velocity skewness and wave boundary layer streaming is also represented. These (and other)
173 processes can generate a net transport in the direction of (or against) wave travel, even in the absence of a local
174 current.

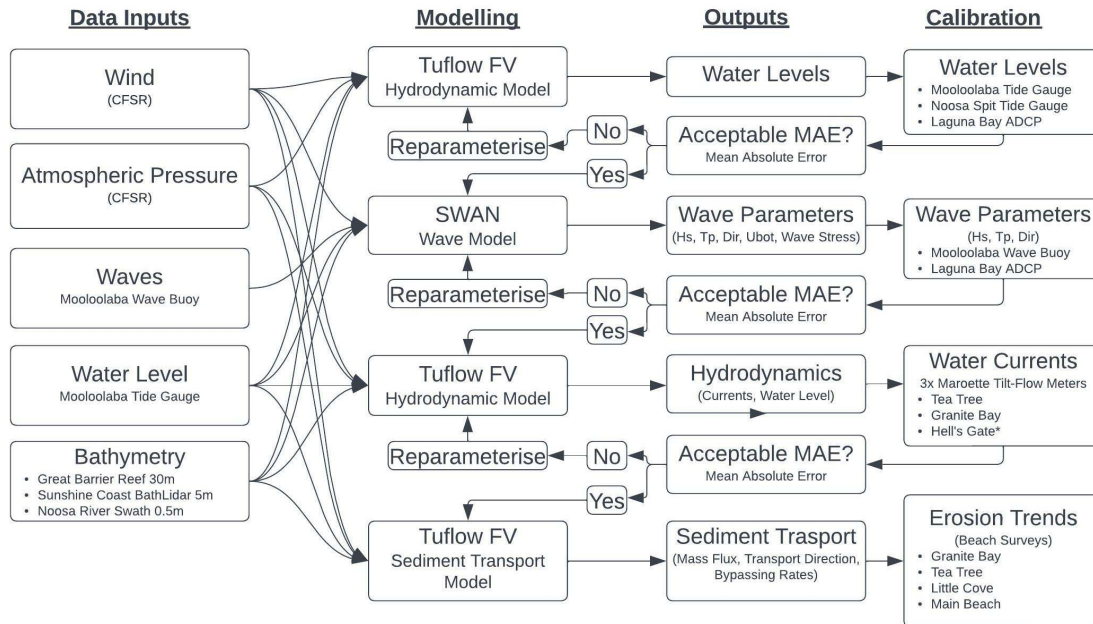
175 3.2 Data collection for model calibration/validation

176 For calibration of the coastal process model, current data was available from several locations around the headland
 177 for a study period that included a range of wave conditions assumed to promote nearshore sediment transport. The
 178 coastal process model was developed in two stages, with the wave model originally developed for a previous piece
 179 of research (Wishaw et al., 2020) and calibrated using data recorded by a bottom-mounted (approx. 9m depth)
 180 acoustic-doppler current profiler (ADCP) in Laguna Bay. An existing hydrodynamics model developed for a project
 181 focusing on the Noosa River estuary (Barnes et al., 2019) used water level and current recordings from the same
 182 ADCP deployment for model development and calibration purposes. This existing hydrodynamic model domain was
 183 retained for the work described herein, however the model mesh was modified with higher resolution added to the
 184 nearshore open coast areas of interest. Three Maroette tilt-flow current meters (Marine Geophysics Laboratory,
 185 2022) were deployed around Noosa Headland to further validate the model results in the study area. The tilt-flow
 186 current meters were deployed in a shallow water (approximately 8m) near three of the headland apexes (**Figure**
 187 **1(b)**) from 1/12/2020 where they were able to collect both modal and storm conditions. Failure of the current meters
 188 was an issue, with current meters breaking and being lost, although fortunately retrieved from nearby beaches for
 189 two of the three current meters, with the Hell’s Gate current meter not retrieved.

190 3.3 Model calibration/validation results

191 Model validation was undertaken for the period 1/12/2020 to 18/12/2020, with the Granite Bay period limited to
 192 15/12/2020 before device failure. The model validation period captured a range of conditions, with smaller modal
 193 wave conditions and a strong wave event emanating from a tropical low in the coral sea that produced wave heights
 194 with an approximate annual recurrence interval of one year. The validation period was curtailed due to instrument
 195 failure; however, the peak of the wave event was captured on retrieved data for both Dolphin Point and Granite Bay
 196 sites. However, the model validation period was sufficient to capture a sufficiently representative range of
 197 conditions when compared with the total wave climate (**Figure 6**). A full list of the calibration parameters can be
 198 found in appendix 1, while the modelling workflow is provided in **Figure 3: Coastal process model modelling**
 199 **workflow** **Figure 3**.

201



202

203 **Figure 3: Coastal process model modelling workflow**

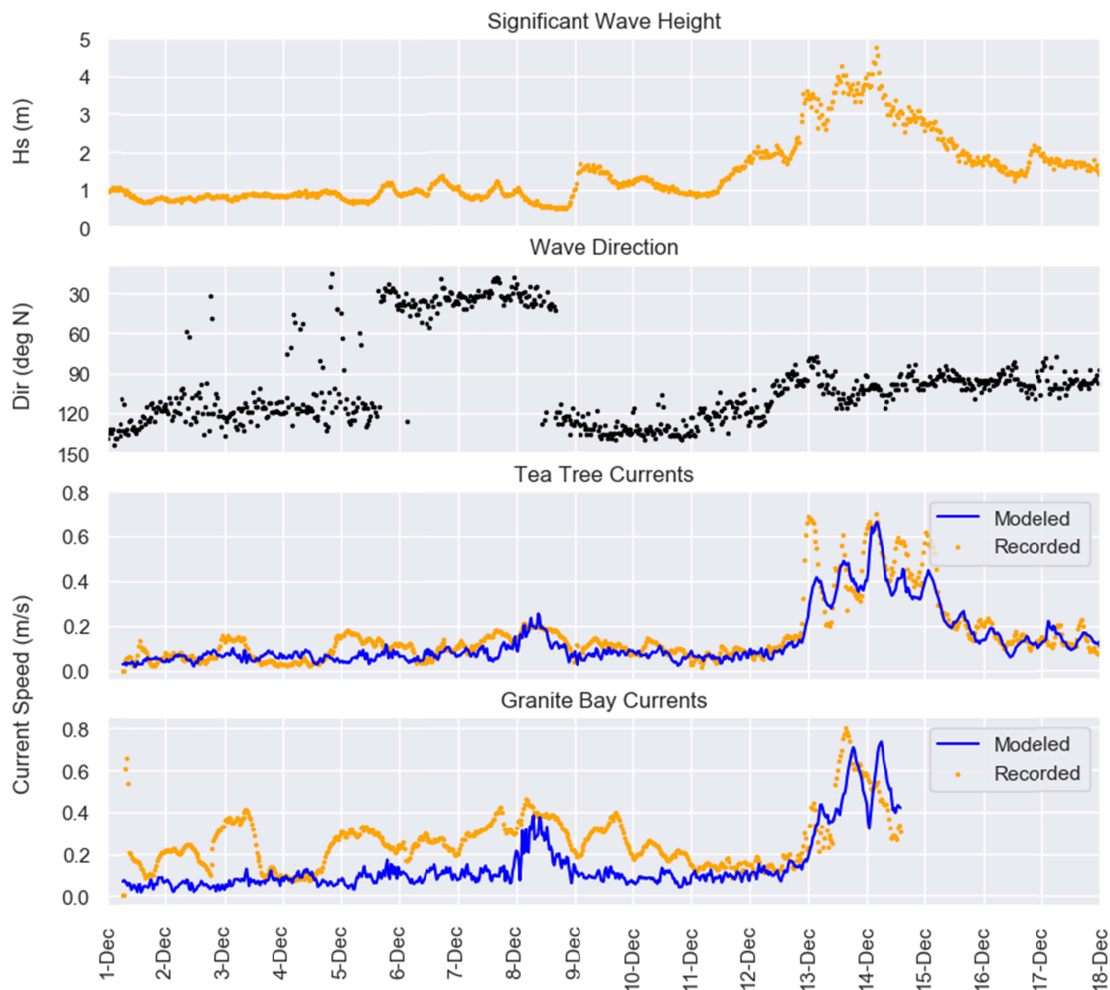
204

205

206 Wave height and direction are provided as well as recorded and (depth-integrated) modelled currents in **Figure 4**.

207 Model skill was assessed by calculating bias, R^2 and Mean Absolute Error (MAE), the results of which are displayed

208 in Table 1. The model shows good skill with reproducing the observed currents, with peak current velocity
 209 magnitude and timing generally well produced. Model results from Dolphin Point show that the magnitude of the
 210 peak currents on 13/12/2020 and 15/12/2020 were underrepresented, during a period where wave direction rapidly
 211 transitions from a southeast direction to a north-northeast direction. Given that the wave input data is only
 212 representing the peak wave direction, it is likely that a multi-directional wave climate is influencing the recorded
 213 currents but is not being adequately resolved in the modeled data, which has been observed in previous headland
 214 bypassing studies (e.g.(Vieira da Silva et al., 2016) that used the full spectrum as boundary conditions. While a
 215 multi-modal input, or the full spectrum, such as Wave-Watch 3 could have been used to inform the wave boundary
 216 condition, the development of the approximation tool is intended to be implemented using easy to access open-
 217 source data, and as such the wave buoy data was used. Despite this limitation, the model is still resolving the
 218 currents well with a high R^2 and low MAE and Bias for the two locations, with Dolphin Point performing better than
 219 Granite Bay, particularly for low current speed conditions. Moreover, under lower current conditions significantly
 220 less sediment is transported. Given the limitations of the model design, particularly with a model bathymetry that is
 221 derived from a 2011 bathymetric survey, the model results are satisfactory for the purposes of this research.
 222



223

224 **Figure 4** : Validation data for the period 01/12/2020 to 18/12/2020 with recorded significant
 225 wave height (top), wave direction (second top), currents at the Dolphin Point site (third top) and
 226 currents at the Granite Bay site (bottom).
 227

228 Table 1: Model validation statistics for Dolphin Point and Granite Bay locations.
 229

Location	N	BIAS (m/s)	MAE (m/s)	R ²
Dolphin Point	899	-0.03	0.05	0.92
Granite Bay	684	-0.12	0.14	0.71

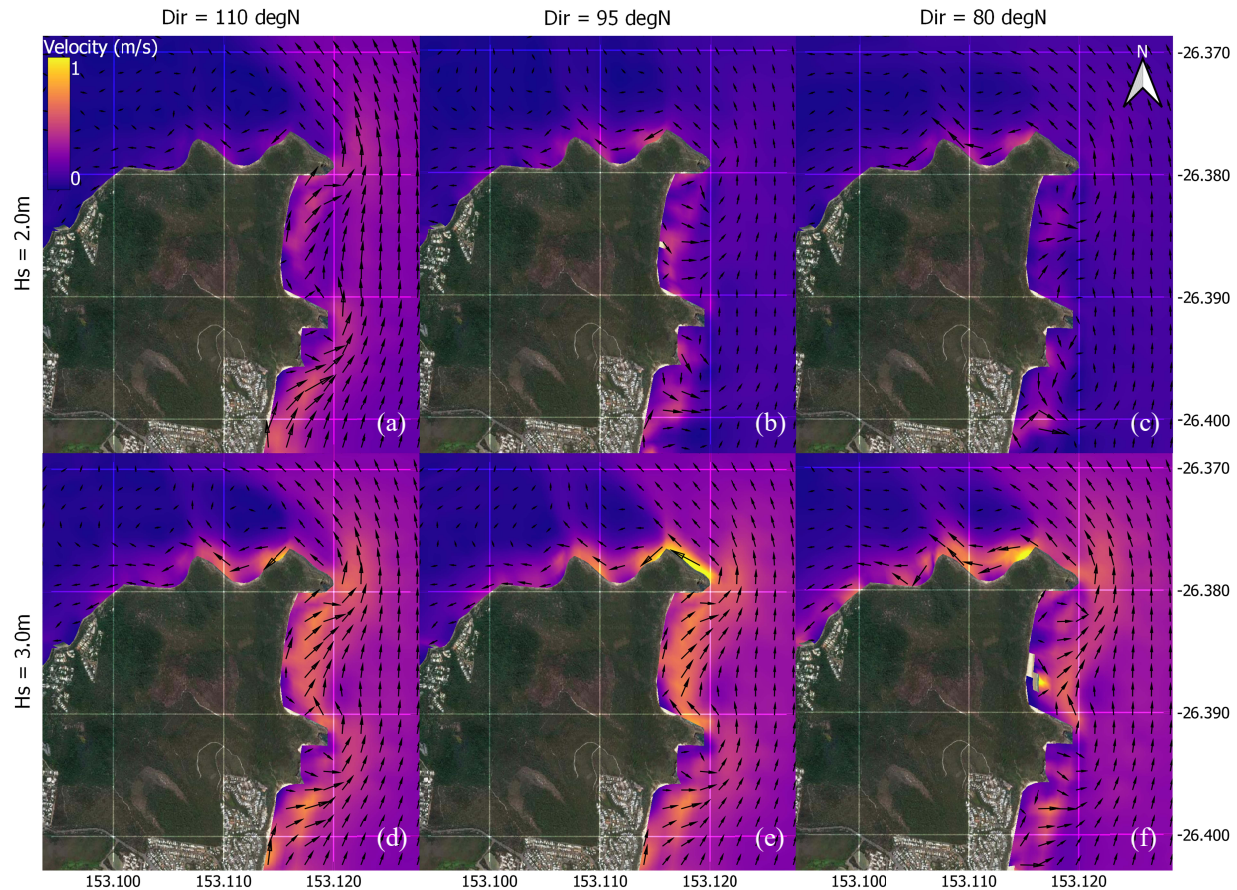
230

231 3.4 Modelled sediment transport and headland bypassing

232 Calibration of coastal process models with respect to sediment transport rates is difficult, due to the large spatial area
 233 of the model domain, variability of transport rates under different forcing and the challenges in doing field work
 234 during events that would be useful to the calibration period. Other studies have utilized a Helley-Smith sampler
 235 (Helley and Smith, 1971) to measure bedload transport rates for calibration of the numerical model, which required
 236 a substantial investment in equipment and expertise to carry out (Vieira da Silva et al., 2016). Despite this, the
 237 Helley-Smith was developed for use in rectilinear flow conditions and is not particularly accurate in complex flow
 238 environment as deviations in the angle of flow to the mouth of the sampler can cause recirculation within the
 239 instrument and reduce the sampling efficiency, without any plausible way to correct for these current deviations
 240 (Gaudet et al., 1994). Consequently, we used survey data that was previously collected (Wishaw et al., 2020) to
 241 assess the order of magnitude of sand migration within the coastal compartments between headland apexes to assess
 242 the performance of the sediment transport model across the period from 20/02/2019 to 28/02/2019. The results
 243 indicate good alignment between the sediment transport model and the observation of erosion and accretion, with
 244 higher levels of erosion in the outer compartments and net deposition in the more protected compartments. At
 245 Dolphin Point, sediment transport was higher than the survey data would suggest, but a review of the model outputs
 246 shows a sediment transport split at this location, with transport remaining attached to the headland and also being
 247 deflected north (**Figure 6**).

248

249 The process-based model illustrates the sensitivity of the nearshore coastal processes to variation in wave height and
 250 direction, particularly around the 2.5m significant wave height threshold previously hypothesized (**Figure 5**). Waves
 251 from the southeast set up longshore transport along the exposed coast south of the headland, resulting in bypassing
 252 of the easterly orientated headland apexes even at lower wave heights (**Figure 5a**). Larger waves with a south-east
 253 orientation produce more energetic bypassing of the eastern points, with sediment freely transported toward the
 254 northern apex of the headland, where current velocities decrease behind the headland apex, allowing for sediment
 255 deposition, or continue north, becoming detached from the headland completely and transporting sand in a cross-
 256 embayment pathway (**Figure 5d**). Smaller waves approaching from the mean wave direction of 95 degrees (east)
 257 produce limited transport around the headland (**Figure 5b**), with larger waves creating strong sediment transport
 258 conditions along the northern side of the headland (**Figure 5e**). Larger waves with a northeast orientation energise
 259 the northern compartments of the headland, but without the strong transport from Hells Gate to Granite Bay seen in
 260 the east conditions (**Figure 5f**).



261

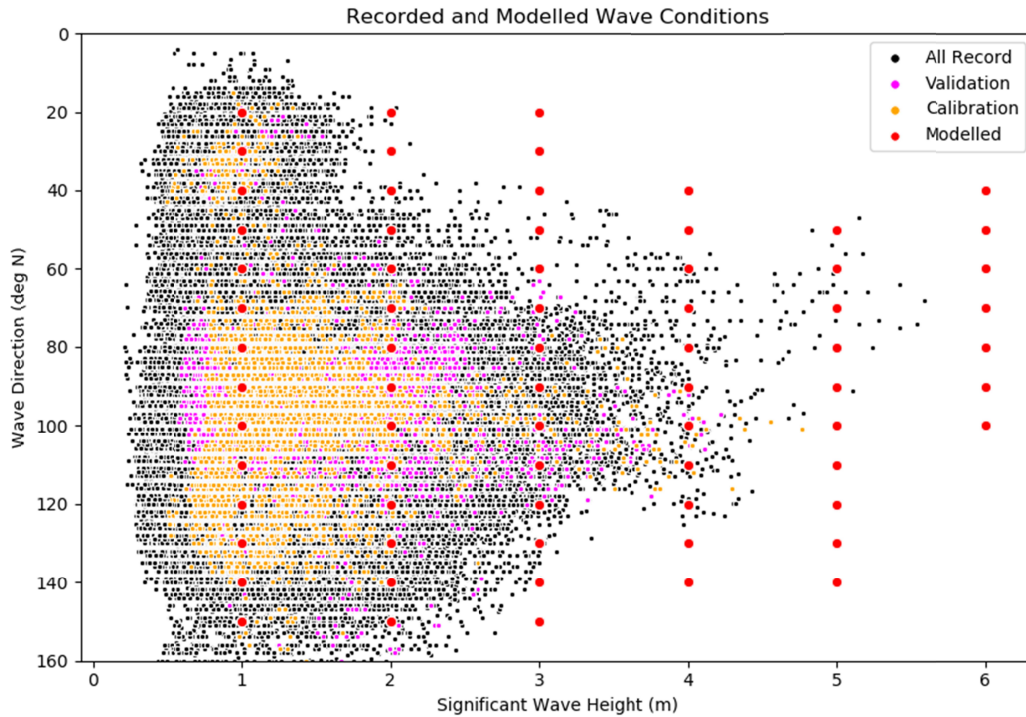
262 **Figure 5:** Sensitivity of nearshore current velocity to variation in the wave climate.263 **4. Headland Bypassing Approximation Tool**264 **4.1 Tool development**

265 While the process model described above was relatively computationally efficient, the use of a process model for
 266 time frames longer than a few months becomes impractical from both a computation and data storage and processing
 267 requirement. As such, a method of schematization of the model inputs was desirable to assess wave conditions for
 268 periods of years to decades. Several methods were reviewed for implementation (Benedet et al., 2016), with
 269 methods such as the ‘Energy Flux Method’ used in other headland transport investigations (Vieira da Silva et al.,
 270 2021). For this research, a Fixed Bin approach was taken, whereby available directional wave data was used to
 271 describe the wave conditions and the model simulated conditions that bounded observed wave conditions (**Figure**
 272 **6**). The model simulations were run with bin sizes of 10 degrees and 1m for wave direction and wave height, which
 273 were then linearly resampled and interpolated to 1 degree and 0.1 meters respectively. Wave period was also
 274 evaluated in an initial test of the tool, with wave period bin sizes of 2 seconds, however, this did not significantly
 275 improve the accuracy of the results but did significantly increase the number of required simulations and the
 276 complexity of the tool. Consequently, wave period was parameterized by taking an average wave period for each
 277 wave height, resulting in a total of 86 bins. While this is significantly higher than the target for the Energy Flux
 278 Method, the Fixed Bin approach was preferred as it provided more evenly distributed points that allowed for more
 279 accurate interpolation and therefore higher resolution across all possible wave conditions.

280

281 A relationship between offshore wave conditions at the Mooloolaba wave buoy and sediment transport at each
 282 headland apex (**Figure 1**) was established and loaded into a database to create the Headland Bypassing
 283 Approximation Tool (HBAT). The accuracy of the sediment bypassing estimates from the HBAT was calibrated

284 against a period simulated in the calibrated process-based model, using daily averaged sediment transport volumes.
 285 The calibration period was between 01-02-2019 to 31-03-2019 that contained large wave conditions from Tropical
 286 Cyclone Oma and overall represented a wide variety of potential wave conditions (**Figure 6**). A calibration factor
 287 was applied for each headland apex to ensure a suitable match between the HBAT results and the process-based
 288 model results and validated against the period 01-12-2020 and 31-01-2021 which contained a diverse range of wave
 289 conditions, including large waves.
 290

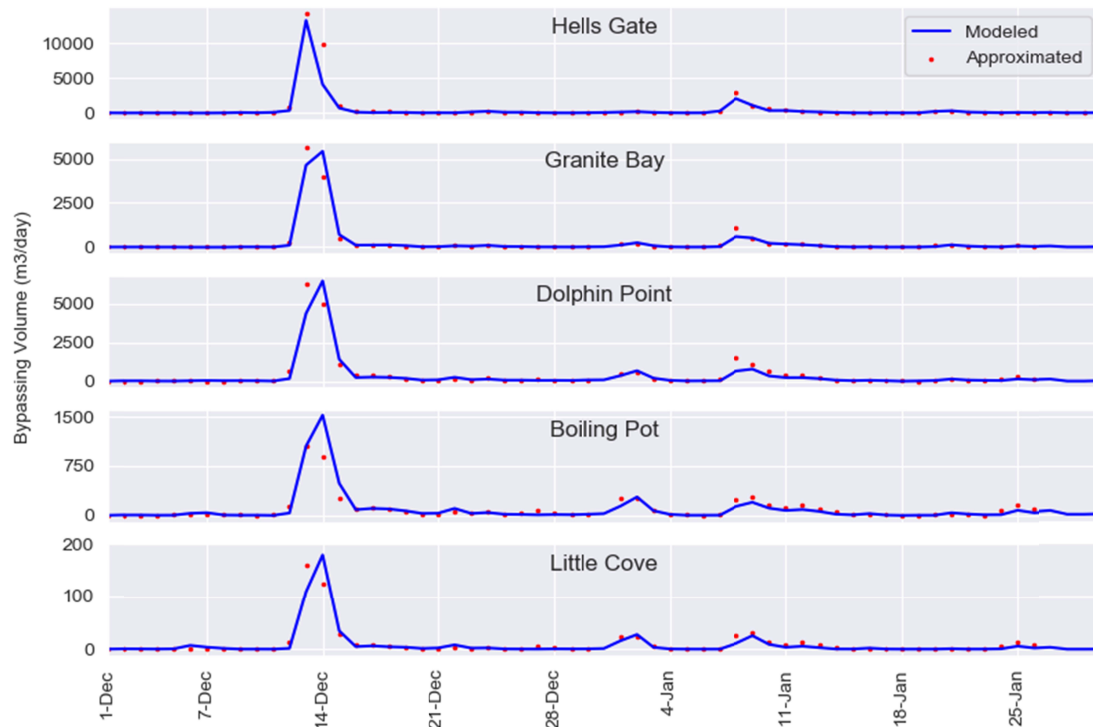


291

292 **Figure 6:** Recorded daily wave conditions for all records at the wave buoy (black), for the
 293 Tropical Cyclone Oma period (orange), the Tropical Cyclone Oma validation period and
 294 modelled wave conditions (red).

295 4.2 Tool validation

296 Validation of the HBAT was undertaken for a 91-day period from 30/11/2020 to 01/03/2021, aligning, with some
 297 some extension, with the validation period for the process based model above and including a variety of wave conditions.
 298 The results showed excellent skill at reproducing the bypassing volumes from the process-based model (**Figure 8**)
 299 with a mean R^2 value for each location equal to 0.9. The model uses a simplified wave-period relationship to reduce
 300 complexity, although testing of this approach indicated that there was limited impact on the daily bypassing
 301 volumes. The validation results indicate a good match between the two datasets, although the model tends to over-
 302 estimate bypassing for large conditions at Boiling Pot. The results are overall excellent, especially considering the
 303 very significant improvement in computational efficiency compared with the process-based model.
 304



305

306 **Figure 7:** Validation of the HBAT against the process-based numerical model. The HBAT (red
 307 dots) shows a strong similarity with the process-based model for most conditions, with some
 308 underestimation of bypassing at Boiling Pot.

309 5. Headland Bypassing Assessments

310 5.1 Assessment scenarios

311 Bypassing sensitivity at each of the headland apexes was evaluated for wave parameters (wave height, wave
 312 direction) as well as climatic drivers that influence wave formation in the Coral and Tasman Seas. Climatic drivers
 313 included the medium-term trends of ENSO phase and seasonality and transient trends derived from the regional
 314 synoptic modality including storminess and synoptic type. Each of these variables was assessed using the full
 315 recorded period of directional wave data from the Mooloolaba Wave buoy (2006-2022).

316

317 Changes in headland bypassing due to changes in wave height and direction were assessed using the HBAT to
 318 understand the sensitivity of headland bypassing to changes in these parameters. Within this evaluation, the relative
 319 bypassing rates of the headland apexes were evaluated, with particular focus on the long term mean wave direction.
 320 A further visual evaluation of the near-shore current set up was undertaken using outputs from the process-based
 321 model around the wave height and directions identified in the previous study (Wishaw et al., 2021). The overall
 322 wave climate was separated into modal and storm conditions based on the approach of Mortlock and Goodwin
 323 (2015), although simplified with respect to storm thresholds. Mortlock and Goodwin assessed the wave threshold
 324 values for separation between modal and storm conditions for southeast Australia and concluded that the H_{s10} value
 325 serves as a reasonable approximation of this boundary. Based on the Mooloolaba wave buoy recordings available to
 326 this study, the H_{s10} value is 2.1m for summer and 1.75m for winter. Wave heights above this threshold were defined
 327 as 'storm' conditions, while wave heights under this threshold were considered 'modal' and further grouped. This
 328 grouping utilised a k-means clustering algorithm to identify clusters within the Mooloolaba wave data and assess
 329 regional synoptic dissimilarity from long term trends.

330

331 Several previous studies have identified that changes in inter-annual or multi-decadal climatic indices can result in
 332 changes to shoreline orientation around headland features, as a consequence of changes to headland bypassing

333 patterns (Goodwin et al., 2013; Mortlock and Goodwin, 2016; Silva et al., 2021). A previous assessment of the
334 relationship between ENSO phase and beach width change at the study site (Wishaw et al., 2021) concluded that
335 there was a negative correlation between the SOI value and the change in beach width for east facing beaches, while
336 no trend was discernable on the protected beaches due to episodic bypassing. Since the 2021 publication, a further
337 two summers of strong La Niña conditions have been experienced at the site, which is significant given the
338 directional wave data set only commences in 2006, with only one La Niña phase recorded previously.

339
340 For ENSO phase, modality and seasonality, the daily bypassing rates for each headland apex was evaluated across
341 the full period of avialbe data and then compressed to produce an average annual bypassing rate for each condition,
342 as both the prevalence and power of each condition are significant in bypassing.

343 5.2 Synoptic Clustering

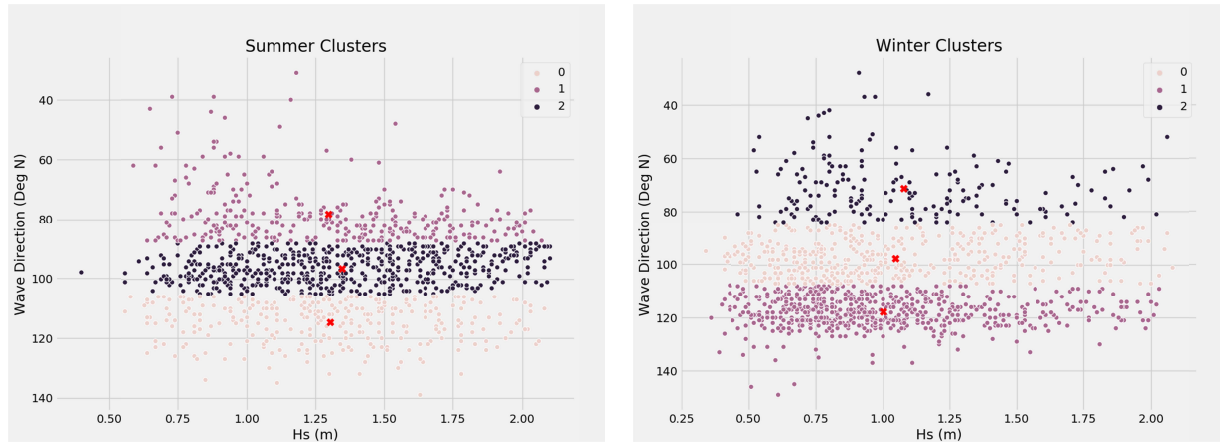
344 Waves impacting the east coast of Australia are generated in a limited number of wave generation zones due to the
345 sheltering of eastern Australia by New Zealand to the east and southeast and several tropical islands to the northeast.
346 These wave generation zones include the Tasman and Coral Seas and a South-Pacific window between New
347 Zealand and the tropical islands (Paula da Silva et al., 2021). Within these wave generation zones, waves are
348 primarily generated by a number of specific synoptic patterns that have been previously described by Mortlock and
349 Goodwin (2015). The work by Mortlock and Goodwin used wave buoys as far north as Brisbane in their evaluation,
350 which we have extended further northward to the Mooloolaba buoy, given the significant sheltering of southerly
351 wave conditions by Mulgumpin (Moreton Island).

352
353 To derive the synoptic conditions that generate modal conditions for the study site, an iterative process was adopted
354 using a k-means clustering algorithm and the generation of synoptic difference plots for each derived cluster. The k-
355 means clustering algorithm is a non-hierarchical clustering method that seeks to find the optimal Voroni cells in
356 multidimensional datasets for 'k' clusters and returns a centroid for each cluster (Dabbura, 2018). The clusters are
357 determined by minimising the sum of dissimilarities between each object and the centroid for the cluster. The
358 minimum dissimilarity will be obtained with 'k' equal to the total number of data points (n) (i.e. where each data
359 point is its own cluster), which is not desirable. Techniques such as the 'elbow' method can be used to identify 'k'
360 numbers that are placed at an inflection in the diminishing returns of dissimilarity between 'k' equals 1 and 'k'
361 equals 'n'.

362
363 For the Mooloolaba data, the model was trained on significant wave height, peak period and peak wave direction for
364 waves under the storm threshold. Using the 'elbow' method, significant inflections were identified between 'k'
365 equals 2 and 'k' equals 6, with a long tail distribution thereafter. For all variations of 'k', the groups split on wave
366 direction only, as wave height and wave period could not sufficiently delineate independent clusters, a result
367 that was previously found by Mortlock and Goodwin.

368
369 From each of these clusters a synoptic dissimilarity plot was produced and evaluated to determine if there is a
370 suitable synoptic explanation to the wave condition. To do this, synoptic pressure across the area of interest for each
371 day within a cluster is averaged to produce an average synoptic condition for the cluster, which is then subtracted
372 from the mean long-term (1991 to 2020) synoptic pressure to derive the synoptic anomaly (NOAA, 2022). This
373 process was undertaken for each group of clusters between $k = 2$ and $k = 6$, with the best results produced where
374 $k=3$, in line with the results from Mortlock and Goodwin (2015). The final clusters that were derived included
375 tightly grouped eastern and south-eastern clusters with more dispersed and slightly less energetic northeast clusters
376 (**Figure 8**).

377
378
379
380



381 **Figure 8:** Mooloolaba wave buoy derived clusters for both (a) summer and (b) winter.

382

383 The clusters (Table 2) produced strong synoptic difference plots (**Figure 9**), with generally stronger synoptic
 384 anomalies in the winter than in the summer. Northeast wave conditions are shown to be the result of a low-pressure
 385 trough over Eastern Australia and a blocking high pressure over New Zealand. Easterly wave conditions in summer
 386 do not show a strong anomaly, suggesting that similarity with the mean long term synoptic state, while in winter a
 387 stronger high-pressure anomaly east of New Zealand is present with a weak southern Tasman low pressure anomaly.
 388 Southeast wave conditions are produced by a central Tasman Low, zonal circulation pattern with high pressure over
 389 southeast Australia and central Pacific. The synoptic anomalies derived for the Mooloolaba site shows strong
 390 similarities with other locations along the east coast of Australia (Mortlock and Goodwin, 2015), with a noticeable
 391 absence of synoptic patterns in the southern ocean that produce southerly wave conditions.

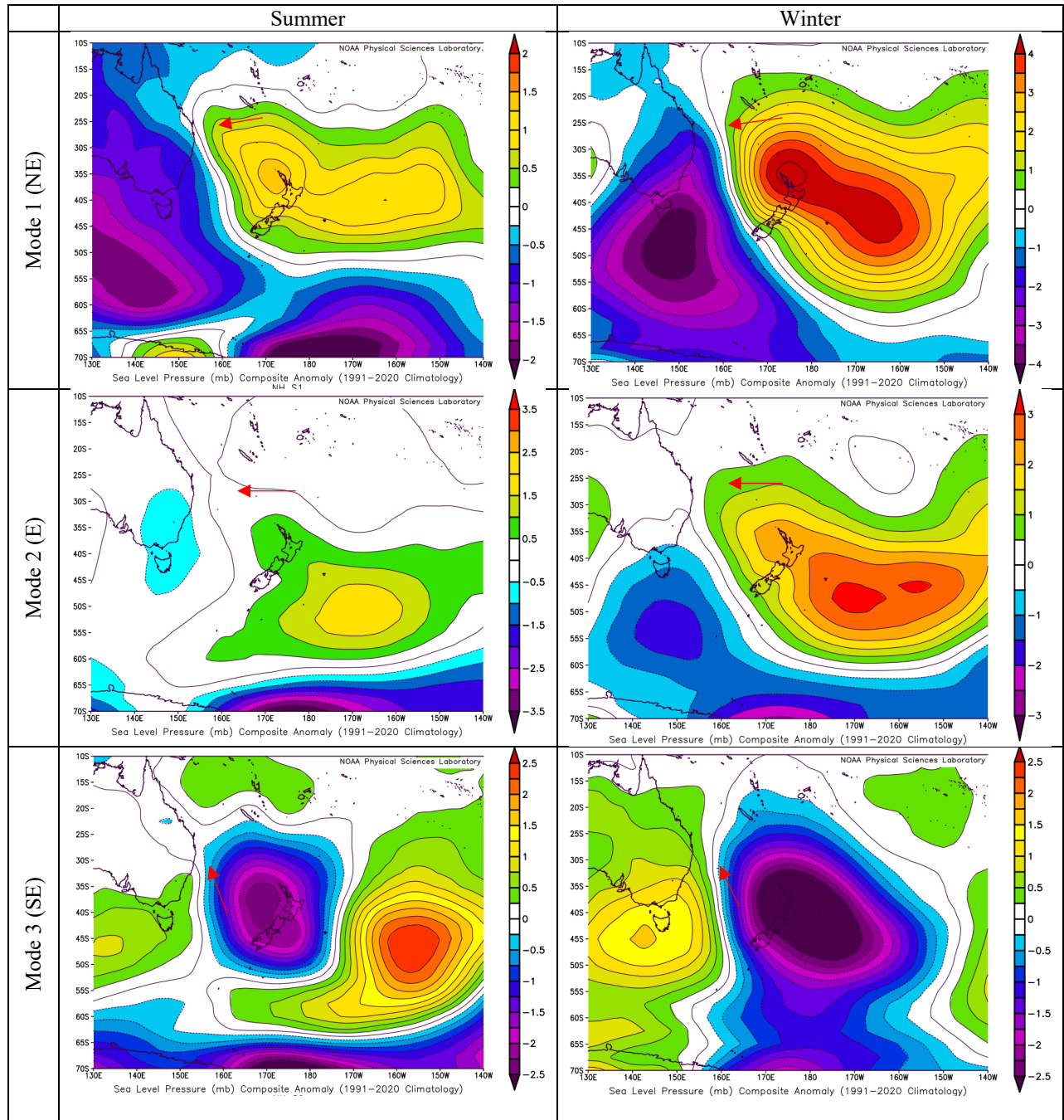
392 Table 2: Modal cluster statistics

393

Season	Mode	Hs Centroid	Dir Centroid	Tp Centroid	Season prevalence
Summer	Mode 1	1.27	76.1	7.7	28%
Summer	Mode 2	1.31	95.1	8.9	51%
Summer	Mode 3	1.27	113.8	9.3	21%
Winter	Mode 1	1	71.4	7.7	14%
Winter	Mode 2	0.98	97.5	9.8	34%
Winter	Mode 3	0.95	117.7	10.6	51%

394

395

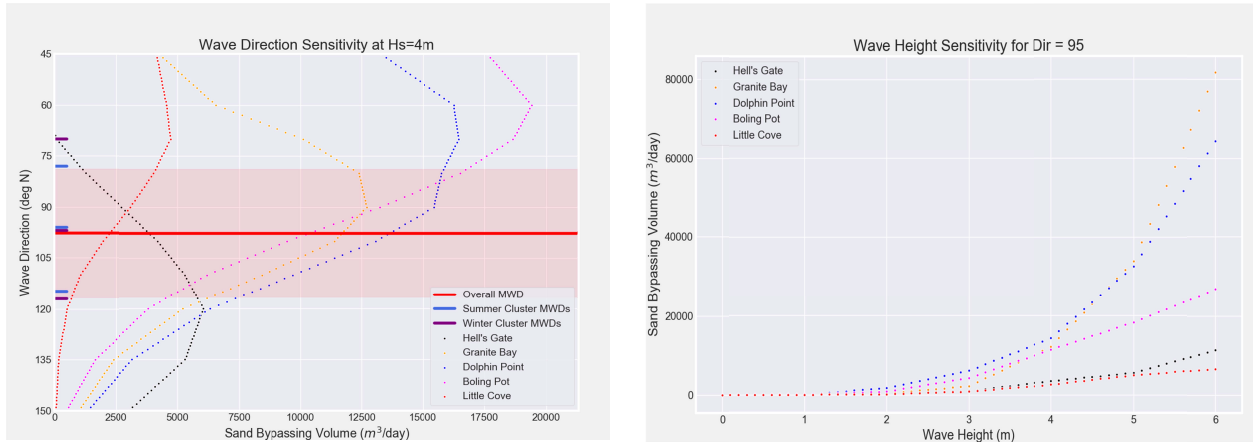


396 **Figure 9:** Synoptic dissimilarity plots for the derived clusters for the Mooloolaba Wave buoy
 397 (NOAA, 2022). These are derived by averaging the synoptic pattern from all days in each cluster
 398 and subtracting from the long term average synoptic conditions. Red arrows indicate swell
 399 direction from the synoptic anomaly towards the study site.

400 **5.3 Headland Bypassing Sensitivity**

401 Headland bypassing rates were shown to be sensitive to both wave direction and wave height (**Figure 10**).
 402 Bypassing sensitivity exhibited an exponential increase in sediment transport with wave height, with low bypassing
 403 rates when the significant wave height was less than 2m (the typical range of ‘modal’ conditions). The headland

404 apex that was orientated to the east (Hell's Gate) showed peak bypassing rates when the wave direction was equal to
 405 120 degrees (southeast), while the north facing points had peak bypassing rates between 70 and 85 degrees
 406 (northeast). This range of wave directions is consistent with the boundary of the first standard deviation of wave
 407 direction for the site and aligns with the mean wave directions of the clusters described in the previous section. As
 408 such, the existing wave climate exists in a 'goldilocks' zone, where both east facing apices and north facing apices
 409 are efficiently activated to ensure bypassing around the whole headland.
 410



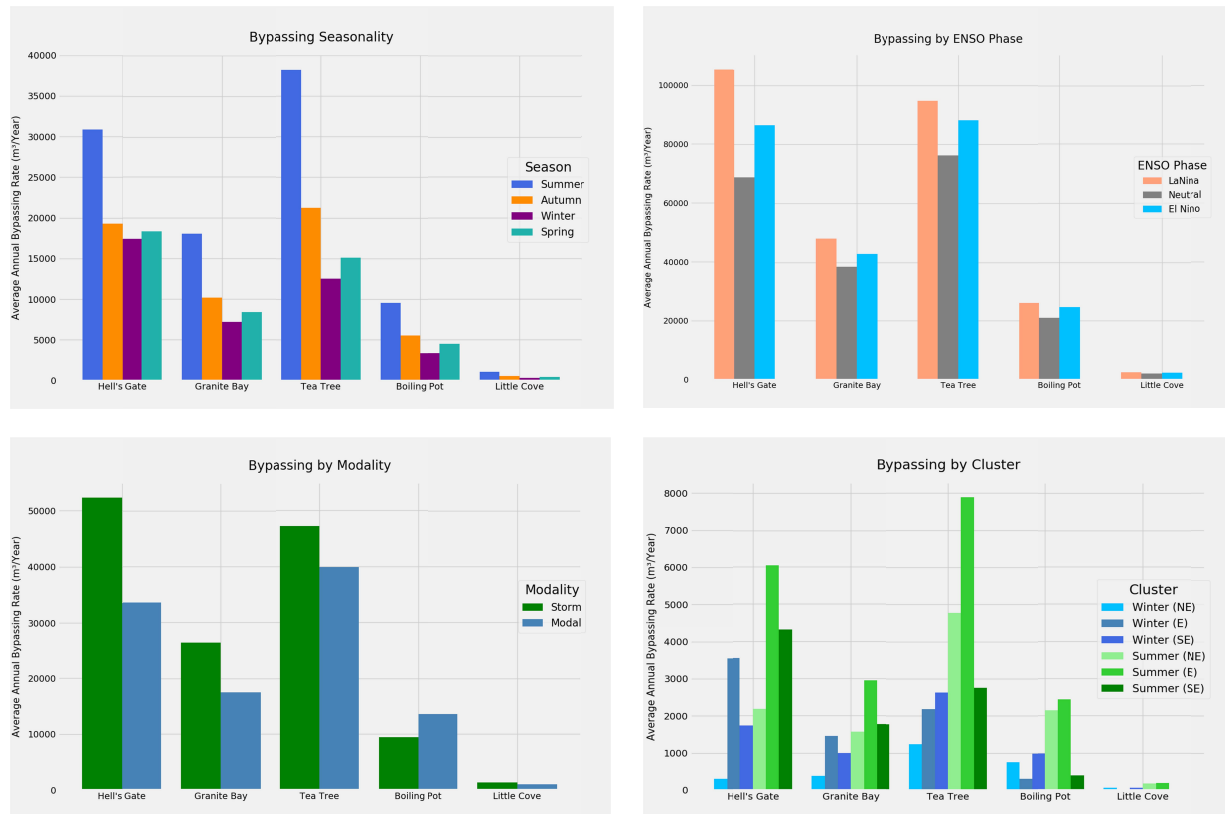
411

412 **Figure 10:** Daily bypassing rates at (a) $H_s=4\text{m}$ including the mean wave direction with a 1
 413 standard deviation buffer and (b) wave direction = 95 degrees approximately at the mean wave
 414 direction.
 415

416 An assessment of climatic conditions that may modulate the wave conditions was undertaken for seasonality, ENSO
 417 phase, modality, and synoptic clusters (**Figure 11**). It is evident that summer is the most active season for headland
 418 bypassing, mostly due to the presence of tropical low and tropical cyclones in the Coral Sea that provide east and
 419 northeast wave energy. Winter was the weakest season for bypassing at all sites, with autumn and spring transitional
 420 between the two extremes.
 421

422 La Niña conditions exhibited higher bypassing rates than El Niño or ENSO neutral conditions, with the relative
 423 increase higher at Hell's Gate, where there is more influence from southeast wave conditions. However, there is a
 424 relatively short record of wave conditions compared with the number of El Niño or La Niña events, and strong
 425 variability within these samples, with the relationship between ENSO phase and bypassing volume not being
 426 statistically significant. Storm conditions (6% of recorded days) provide a larger proportion of the bypassing at the
 427 most headland apices, except for Boiling Pot. The deep seabed at Hell's Gate, Granite Bay and Dolphin Point
 428 requires larger waves to initiate transport, while a shallower seabed at Boiling Pot will facilitate greater sensitivity to
 429 smaller wave conditions, while combined with the greater prevalence of these conditions (94% of recorded days)
 430 results in Boiling Pot being influenced by modal conditions more than storm conditions.
 431

432 Of the various synoptic patterns derived for Noosa that influence modal wave conditions, the summer clusters
 433 dominated for overall sediment bypassing volume at all locations. For both winter and summer, the synoptic
 434 conditions that resulted in easterly wave conditions were the most significant, with the northeast sector in summer
 435 also significant for the headland apices on the north side of the headland.
 436



437

438 **Figure 11:** Influence of climatic drivers on bypassing rates for all headland apexes at Noosa
 439 Headland including (a) seasonality, (b) ENSO phase, (c) modality, and (d) regional synoptic
 440 conditions.

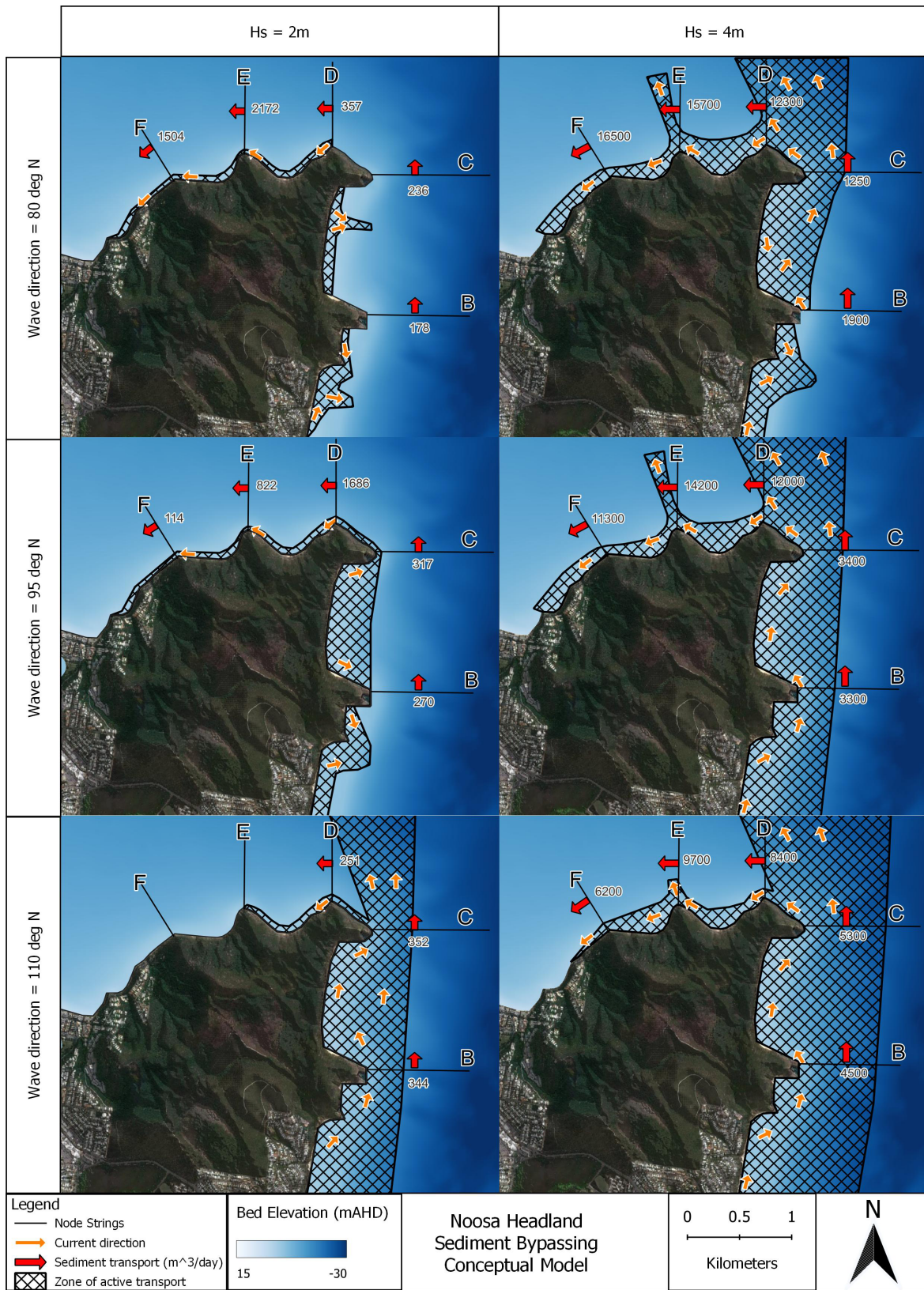
441 6. Discussion

442 Coastal processes around headlands present an interesting challenge for researchers and coastal managers alike, as a
 443 detailed comprehension of the coastal processes requires the use of specialist modelling, which is intensive to
 444 develop, calibrate and implement, particularly over long study time frames. Nevertheless, the results are critical for
 445 understanding the availability of sediment at downdrift beaches. Our results from a Noosa Headland case study
 446 show that detailed coastal process models can be developed and used to calibrate an approximation tool that is
 447 capable of reproducing headland sediment bypassing rates with a high degree of accuracy, while also capable of
 448 being used with readily available datasets and lower technical expertise. This approximation tool has been utilised to
 449 investigate an extensive dataset (16 years) of coastal data to develop a better understanding of headland sediment
 450 bypassing with respect to wave climate and regional climatic variability.

451 6.1 Headland Bypassing Pathways

452 Previous research at this site (Wishaw et al., 2021) developed a conceptual understanding of bypassing of the
 453 headland, that this research has expanded into a complete understanding of nearshore coastal processes. The
 454 previous work hypothesized bypassing to occur under moderate wave forcing via the migration of large 'sand slugs',
 455 and while this remains valid, a more comprehensive understanding of sediment transport pathways has been
 456 illuminated in this research (**Figure 12**).

457



458

459
460

Figure 12: Noosa Headland sediment bypassing conceptual model.

461 The two pathways for sand migration around the headland are a nearshore attached pathway and a cross-embayment
462 pathway. The nearshore attached pathway behaves as previously hypothesized, with wave breaking energizing the
463 nearshore environment and continuously moving sediment around the headland. The cross-embayment pathway
464 shows that sediment transport can become detached from the headland and migrate across the embayment to the
465 north of the headland (Laguna Bay), a conclusion also found at other headlands (Goodwin et al., 2013). Of particular
466 interest, this cross-embayment pathway was not only set up at the largest apex of the headland (Hell's Gate), where
467 there is considerable updrift distance to energise a longshore current that can transport the sediment into this cross
468 embayment, but also at Dolphin Point, a minor apex with less set-up distance for currents to form. The sediment that
469 enters the cross-embayment pathway at Hell's Gate moves into water that is up to 20m deep, while sediment from
470 Dolphin Point follows a pathway across an area where the seabed is between 10m and 12m, suggesting that this
471 sediment may remain available as a sand source for the northern area of the headland under suitable conditions.
472 Sediment moving through this cross-embayment pathway, from either headland apex, settles out in Laguna Bay as
473 the currents dissipate, resulting in the seabed updrift of the headland being significantly thicker with nearshore
474 sediments (Jones and Stephens, 1981) and much shallower than downdrift locations at a similar distance from the
475 shoreline. As a result of continuous energizing by wave breaking, the nearshore attached pathway is the faster mode
476 of transport from the headland apex to the downdrift beaches north of Noosa River.
477 The results of this study indicate that there are also two 'modes' of bypassing of the headland, with the previously
478 hypothesized 'sand slug' mode occurring with sufficient wave forcing, generally considered to be when $H_s > 2.5\text{m}$,
479 and a smaller magnitude 'trickle' bypassing occurring under smaller wave conditions ($1\text{m} > H_s < 2.5\text{m}$). This wave
480 height threshold aligns with the regional definition of 'storm' conditions and 'modal' conditions that has a statistical
481 boundary at $H_s = 2.1\text{m}$ for summer wave and 1.75m for winter waves. Despite the 'storm' conditions providing
482 significantly more energy to the nearshore environment, they only account for approximately 6% of days at the site,
483 while the modal conditions that force the 'trickle' bypassing make up the vast majority of days at the site. The 'sand
484 slug' mode that occurs under 'storm' conditions makes up approximately 60-70% of total bypassing by volume for
485 the exposed headland apexes to the east of Noosa Headland, while the more protected headlands on the northern side
486 of the headland show an increasing proportion of 'trickle' bypassing, due in large part, to the shallower sea bed at
487 these apexes.

488 6.2 Influence of regional climate drivers

489 The relationship between regional climate conditions and sediment bypassing at each headland apex was directly
490 measurable within this study, with ENSO phase, seasonality, storminess and synoptic modality all assessed. The
491 most significant of these was seasonality, with summer periods producing 80% to 150% more bypassing than winter
492 periods, with spring and autumn being transitional between these two. Summer wave conditions at the site are more
493 northerly orientated and more energetic than winter conditions as the site is exposed to tropical storm and cyclone
494 conditions in the Coral Sea, northeast of the site. During winter, the Coral and Tasman Seas are dominated by extra-
495 tropical low-pressure systems in the Tasman Sea, that produce southerly wave conditions that the site is partially
496 protected from due to offshore islands and the overall shoreline orientation. This is also seen in the synoptic
497 modality, with summer modalities more significant to bypassing than winter modalities. For Hell's Gate, which is
498 fully exposed to waves from all synoptic modes, easterly and southeasterly waves are the most significant, while for
499 the apexes on the north of the headland, synoptic modes which produce easterly and northeasterly wave conditions
500 are the most significant. The significance of storminess was discussed in the previous section, while ENSO phase
501 was only significant for Hells Gate, which aligns with the previous conclusions from the site (Wishaw et al., 2021),
502 due to ENSO phase modulating the modal wave power from southerly synoptic patterns (Mortlock and Goodwin,
503 2016).

504 6.3 Future climate implications

505 Predictions of future wave climate scenarios remain complicated due to the multitude of influencing factors and
506 their complex interaction between each other. At the study site, the wave climate consists of a combination of storm
507 and modal wave conditions from various sources that are all predicted to be influenced by a warming planet. Modal
508 synoptic patterns in the Coral and Tasman Seas are expected to change their relative power in future, due to a
509 southward migration of the sub-tropical ridge that controls the location of these patterns. This change in wave power
510 is the result of the relative weakening of southerly wave forming synoptic modes and strengthening of the easterly
511 wave forming synoptic modes (Mortlock and Goodwin, 2015). Storm waves, typically generated from tropical lows
512 and cyclones in the Coral Sea are likely to change in future climate scenarios, with a poleward migration of

513 maximum cyclone intensity suggested, that would bring wave generation closer to the site (Kossin et al., 2014).
514 Global forecasts of the average wave climate suggests both an increase in overall wave power (Reguero et al., 2019),
515 and a shift in mean deep-water wave direction of between 5–15° by the end of the century (Morim et al., 2019).
516 However, each of these findings are provided in the context of remaining uncertainty of global climate projections
517 and the ability of models to suitably predict changes to such a degree of accuracy that deterministic forecasts of
518 future wave climates can be derived. Nonetheless, with the tools developed in this research we can explore how
519 different scenarios of wave climate modification may influence the study site. Predictions of weakening southerly
520 modes of wave formation and strengthening easterly modes and north-east storm waves would migrate the average
521 wave climate in anti-clockwise direction. This would have the effect of strengthening conditions that create
522 sediment transport on the north side of the headland, while weakening conditions that drive transport on the east
523 side. At present, the wave climate exists in a 'goldilocks' zone where transport volumes on the east and north sides
524 of the headland are slightly skewed towards increased transport on the north side, resulting in net erosion of the
525 beaches on the north side. Predicted changes would enhance this pattern, with increased erosive pressure on the
526 northern beaches, with less sediment transport around the large headland apex at the east of the headland, resulting
527 in increased sand starvation of these beaches.

528 **7. Conclusions**

529 This research developed a tool for accurately forecasting headland sediment transport in a highly efficient manner
530 which was used to explore changes in sediment transport volume with respect to changes in wave conditions and
531 regional climate drivers that control wave conditions. Our findings reveal that headland transport occurs in two
532 different modes; a 'trickle' bypassing mode occurs under conditions with lower wave heights ($H_s < 2\text{m}$) and the
533 migration of large 'sand slugs' under larger wave heights. Despite their difference in transport rate, these two modes
534 can provide similar annual transport volumes due to the greater prevalence of smaller wave conditions. Sediment
535 being transported around the headland was found to follow two pathways; a more energetic headland attached
536 pathway that remained in the shallower area around the headland and a cross-embayment pathway that became
537 detached from the headland and transported sediment into the deep water north of the headland, where transport
538 rates were significantly lower.

539
540 Headland sediment transport was sensitive to changes in both wave height and direction, with different conditions
541 required for sediment transport on the east and north side of the headland. Balanced migration of sediment transport
542 around the headland was reliant on the wave direction remaining between the current mean wave direction and one
543 standard deviation south (15 degrees) of the existing mean wave direction. Seasonality was found to be the most
544 significant climate influence on headland bypassing at the site, with synoptic modality significant for 'trickle'
545 bypassing, where summer synoptic patterns that generated east and northeast waves produced the most bypassing.
546 ENSO phase was only significant for the easterly orientated apexes, with La Niña conditions providing more
547 bypassing than either El Niño or ENSO-neutral conditions, while the strength of this pattern was reduced for
548 northerly orientated headland apexes.

549
550 Finally, the research considered the implications of changing wave conditions under a future climate scenario. While
551 the precise magnitude of this change continues to be developed, this research considered the most likely scenario of
552 an anticlockwise rotation of the wave environment. This change in the wave climate would reduce bypassing of the
553 east face of the headland and increase the transport on the north side, resulting in more frequent sediment starvation
554 of the protected beaches on the north side of the headland.

555

556 **8. Acknowledgements**

557 The authors are grateful for the support and contributions from the University of the Sunshine Coast and the support
558 from BMT commercial. The authors also acknowledge the valuable contribution from the Queensland
559 Government's Department of Environment and Science who have provided data for this research.

560

561

562 **9. Open Research**

563 The modelling input and synoptic clustering data used for the development of the process-based model and the
 564 synoptic clustering outputs in the study are available at the University of the Sunshine Coast Research Bank via
 565 <https://doi.org/10.25907/00751> with open access.

566 **10. References**

- 567
 568 Barnes, M., Cullen, J., O'Malley-Jones, K., 2019. Noosa Spit Shoreline Erosion Management Plan, BMT.
 569 Barnes, M., Huxley, C., Andrews, M., 2013. Sunshine Coast Regional Council - Coastal processes study for the
 570 Sunshine Coast, BMT WBM Brisbane, Australia.
 571 Barnes, M.T., Ian; Wood, Peter; Voisey, Chris, 2015. Assessment of Capital Works Options to Mitigate Shoaling at
 572 the Mooloolaba Harbour Entrance, Australasian Coast & Ports, Auckland, New Zealand.
 573 Benedet, L., Dobrochinski, J.P.F., Walstra, D.J.R., Klein, A.H.F., Ranasinghe, R., 2016. A morphological modeling
 574 study to compare different methods of wave climate schematization and evaluate strategies to reduce
 575 erosion losses from a beach nourishment project. *Coastal Engineering*, 112, 69-86.
 576 BMT Commercial Australia, 2022. TUFLOW 2D/3D Flexible Mesh Modelling.
 577 Dabbura, I., 2018. K-means Clustering: Algorithm, Applications, Evaluation Methods, and Drawbacks.
 578 Delft University of Technology, 2016. SWAN Scientific and Technical Documentation, version 41.10.
 579 Deltares, 2022. X Beach.
 580 Gaudet, J., Roy, A., Best, J., 1994. Effect of orientation and size of Helley-Smith sampler on its efficiency
 581 *Journal of Hydraulic Engineering*, 120(6), 758-766.
 582 George, D.A., Largier, J.L., Storlazzi, C.D., Barnard, P.L., 2015. Classification of rocky headlands in California
 583 with relevance to littoral cell boundary delineation. *Marine Geology*, 369, 137-152.
 584 Geoscience Australia, 2017. High-resolution depth model for the Great Barrier Reef – 30m.
 585 Goodwin, I.D., Freeman, R., Blackmore, K., 2013. An insight into headland sand bypassing and wave climate
 586 variability from shoreface bathymetric change at Byron Bay, New South Wales, Australia. *Marine*
 587 *Geology*, 341, 29-45.
 588 Goodwin, I.D., Mortlock, T.R., Browning, S., 2016. Tropical and extratropical-origin storm wave types and their
 589 influence on the East Australian longshore sand transport system under a changing climate. *Journal of*
 590 *Geophysical Research: Oceans*, 121(7), 4833-4853.
 591 Harris, P.T., Heap, A.D., Bryce, S.M., Porter-Smith, R., Ryan, D.A., Heggie, D.T., 2002. Classification of
 592 Australian Clastic Coastal Depositional Environments Based Upon a Quantitative Analysis of Wave, Tidal,
 593 and River Power. *Journal of Sedimentary Research*, 72(6), 858-870.
 594 Helley, E.J., Smith, W., 1971. Development and Calibration of a Pressure-Difference Bedload Sampler. U.S
 595 Geological Survey.
 596 Jones, M.R., Stephens, A.W., 1981. Sand transport at Noosa. Queensland: Summary, Geological Survey of
 597 Queensland
 598 King, E.V., Conley, D.C., Masselink, G., Leonardi, N., McCarroll, R.J., Scott, T., Valiente, N.G., 2021. Wave, Tide
 599 and Topographical Controls on Headland Sand Bypassing. *Journal of Geophysical Research: Oceans*,
 600 126(8).
 601 Klein, A.H.F., Vieira da Silva, G., Taborda, R., da Silva, A.P., Short, A.D., 2020. Headland Bypassing and
 602 Overpassing: form, processes and applications, *Sandy Beach Morphodynamics*. Elsevier, pp. 814.
 603 Kossin, J.P., Emanuel, K.A., Vecchi, G.A., 2014. The poleward migration of the location of tropical cyclone
 604 maximum intensity. *Nature*, 509(7500), 349-352.
 605 Marine Geophysics Laboratory, 2022. Current Meter: Marotte HS.
 606 McCarroll, R.J., Masselink, G., Valiente, N.G., King, E.V., Scott, T., Stokes, C., Wiggins, M., 2021. An XBeach
 607 derived parametric expression for headland bypassing. *Coastal Engineering*, 165.
 608 Morim, J., Hemer, M., Wang, X.L., Cartwright, N., Trenham, C., Semedo, A., Young, I., Bricheno, L., Camus, P.,
 609 Casas-Prat, M., Erikson, L., Mentaschi, L., Mori, N., Shimura, T., Timmermans, B., Aarnes, O., Breivik,
 610 Ø., Behrens, A., Dobrynin, M., Menendez, M., Staneva, J., Wehner, M., Wolf, J., Kamranzad, B., Webb,

- 611 A., Stopa, J., Andutta, F., 2019. Robustness and uncertainties in global multivariate wind-wave climate
612 projections. *Nature Climate Change*(9), 711–718.
- 613 Mortlock, T.R., Goodwin, I.D., 2015. Directional wave climate and power variability along the Southeast Australian
614 shelf. *Continental Shelf Research*, 98, 36-53.
- 615 Mortlock, T.R., Goodwin, I.D., 2016. Impacts of enhanced central Pacific ENSO on wave climate and headland-bay
616 beach morphology. *Continental Shelf Research*, 120, 14-25.
- 617 NOAA, 2022. Daily Mean Composites.
- 618 Paula da Silva, A., Vieira da Silva, G., Perez, J., 2021. Wave Generation Zones off the East Australian Coast,
619 Australasian Coasts and Ports 2021, Christchurch, New Zealand.
- 620 Queensland Government, 2012. Queensland coastal risk and bathymetric LiDAR: a pilot study for collecting near-
621 shore bathymetry, Queensland Department of Science, Information Technology, Innovation and the Arts,
622 Brisbane, Australia.
- 623 Queensland Government, 2019a. Tide Monitoring Sites.
- 624 Queensland Government, 2019b. Wave Monitoring Sites.
- 625 Reguero, B.G., Losada, I.J., Mendez, F.J., 2019. A recent increase in global wave power as a consequence of
626 oceanic warming. *Nat Commun*, 10(1), 205.
- 627 Saha, S., Shrinivas Moorthi, Xingren Wu, Jiande Wang, Sudhir Nadiga, Patrick Tripp, David Behringer, Yu-Tai
628 Hou, Hui-ya Chuang, Mark Iredell, Michael Ek, Jesse Meng, Rongqian Yang, Malaquias Peña Mendez,
629 Huug Van Den Dool, Qin Zhang, Wanqiu Wang, Mingyue Chen, Emily Becker., 2014. The NCEP Climate
630 Forecast System Version 2. *Journal of Climate*, 27(6), 2185-2208.
- 631 Saha, S.N., C. Thiaw, J. Wang, W. Wang, Q. Zhang, H. M. Van Den Dool, H.-L. Pan, S. Moorthi, D. Behringer, D.
632 Stokes, M. Peña, S. Lord, G. White, W. Ebisuzaki, P. Peng, P. Xie, 2006. The NCEP Climate Forecast
633 System *Journal of Climate*, 19(15).
- 634 Silva, A.P.D., Vieira da Silva, G., Strauss, D., Murray, T., Woortmann, L.G., Taber, J., Cartwright, N., Tomlinson,
635 R., 2021. Headland bypassing timescales: Processes and driving forces. *Sci Total Environ*, 793, 148591.
- 636 Splinter, K.D., Coco, G., 2021. Challenges and Opportunities in Coastal Shoreline Prediction. *Frontiers in Marine
637 Science*, 8.
- 638 Splinter, K.D., Davidson, M.A., Golshani, A., Tomlinson, R., 2012. Climate controls on longshore sediment
639 transport. *Continental Shelf Research*, 48, 146-156.
- 640 Van Rijn, L.C., 2007a. United view of sediment transport by currents and waves I: Initiation of motion, Bed
641 roughness and bed load transport. *Journal of Hydraulic Engineering*, 133(6), 649-667.
- 642 Van Rijn, L.C., 2007b. United view of sediment transport by currents and waves II: Suspended transport. *Journal of
643 Hydraulic Engineering*, 133(6), 668-689.
- 644 Van Rijn, L.C., 2007c. United view of sediment transport by currents and waves III: Graded beds. *Journal of
645 Hydraulic Engineering*, 133(6), 761-775.
- 646 Vieira da Silva, G., Stauss, D., Murray, T., Tomlinson, R., Paula da Silva, A., 2021. Impacts of Climate Change on
647 Sediment Transport Rates Around Burleigh Heads, Australasian Coasts & Ports 2021 Conference,
648 Christchurch.
- 649 Vieira da Silva, G., Toldo, E.E., Klein, A.H.d.F., Short, A.D., Woodroffe, C.D., 2016. Headland sand bypassing —
650 Quantification of net sediment transport in embayed beaches, Santa Catarina Island North Shore, Southern
651 Brazil. *Marine Geology*, 379, 13-27.
- 652 Vieira da Silva, G., Toldo Jr, E.E., Klein, A.H.d.F., Short, A.D., 2018. The influence of wave-, wind- and tide-
653 forced currents on headland sand bypassing – Study case: Santa Catarina Island north shore, Brazil.
654 *Geomorphology*, 312, 1-11.
- 655 Wishaw, D., Leon, J., Fairweather, H., Crampton, A., 2021. Influence of wave direction sequencing and regional
656 climate drivers on sediment headland bypassing. *Geomorphology*, 383.
- 657 Wishaw, D., Leon, J.X., Barnes, M., Fairweather, H., 2020. Tropical Cyclone Impacts on Headland Protected Bay.
658 *Geosciences*, 10(5).

659 Appendix 1 Model Configuration

660 Table 3: SWAN model calibration parameters

Parameter	Value
Model mode	Gen 3
Friction expression	Collins (1972)

Collins bottom friction coefficient	0.015
Numerics	BSBT
dabs	0.02
drel	0.02
curvant	0.02
npnts	98.0
Non-stationary computation	On
mxitns	15
limiter	0.1
DIRIMPL	On
cdd	0.5
Timestep	1.0 hours

661 Table 4: TUFLOW model calibration parameters

Parameter	Value
momentum mixing model	Smagorinsky
horizontal gradient limiter	LCD
bottom drag model	ks
Reference salinity	35.0
Reference temperature	20.0
Reference mslp	1011
Reference density	1025
Density air	1.18
Kinematic viscosity	1.0e-6
global horizontal eddy viscosity	0.2
global vertical eddy viscosity limits	1.0e-4, 9999.0
bottom roughness	0.05
waves	On
Output interval	0.25 hours

662